The FEBS Journal

FEBS PRESS science publishing by scientists

A GUIDE TO...

A guide to sample delivery systems for serial crystallography

Feng-Zhu Zhao[1], Bin Zhang[1], Er-Kai Yan[1], Bo Sun[2], Zhi-Jun Wang[2], Jian-Hua He[2] and Da-Chuan Yin[1,3]

1 School of Life Sciences, Northwestern Polytechnical University, Xi'an, China
2 Shanghai Institute of Applied Physics, Chinese Academy of Sciences, Shanghai, China
3 Shenzhen Research Institute, Northwestern Polytechnical University, Shenzhen, China

Keywords
fixed-target system; in suit diffraction; moving target system; sample delivery; serial crystallography

Correspondence
J.-H. He, Shanghai Institute of Applied Physics, Chinese Academy of Sciences, 239 Zhangheng Road, Shanghai 201204, China
Tel: +027 6875 8256
E-mail: hejianhua@sinap.ac.cn
D.-C. Yin, School of Life Sciences, Northwestern Polytechnical University, 127 West Youyi Road, Xi'an, Shaanxi 710072, China
Tel: +029 8846 0254
E-mail: yindc@nwpu.edu.cn

(Received 11 May 2019, revised 26 September 2019, accepted 15 October 2019)

doi:10.1111/febs.15099

Crystallography has made a notable contribution to our knowledge of structural biology. For traditional crystallography experiments, the growth of crystals with large size and high quality is crucial, and it remains one of the bottlenecks. In recent years, the successful application of serial femtosecond crystallography (SFX) provides a new choice when only numerous microcrystals can be obtained. The intense pulsed radiation of X-ray free-electron lasers (XFELs) enables the data collection of small-sized crystals, making the size of crystals no longer a limiting factor. The ultrafast pulses of XFELs can achieve 'diffraction before destruction', which effectively avoids radiation damage and realizes diffraction near physiological temperatures. More recently, the SFX has been expanded to serial crystallography (SX) that can additionally employ synchrotron radiation as the light source. In addition to the traditional ones, these techniques provide complementary opportunities for structural determination. The development of SX experiments strongly relies on the advancement of hardware including the sample delivery system, the X-ray source, and the X-ray detector. Here, in this review, we categorize the existing sample delivery systems, summarize their progress, and propose their future prospectives.

Introduction

Approximately 100 years ago, a series of important discoveries [in 1912, Max von Laue discovered X-ray diffraction (XRD) in crystals [1]; from 1913 to 1914, William Henry Bragg and William Lawrence Bragg proposed diffraction theory and established Bragg's Law [2]] marked the beginning of analyzing material structure through crystallography. Today, protein crystallography is undergoing a significant change with

Abbreviations
ADE, acoustic droplet ejection; BeV2, picornavirus bovine enterovirus 2; bR, bacteriorhodopsin; CA II, carbonic anhydrase II; CcO, cytochrome *c* oxidase; CoMESH, concentric-flow electrokinetic injector; CPV18, cytoplasmic polyhedrosis virus type 18 polyhedrin; CuNiR, copper nitrite reductase; DFFN, double-flow focusing nozzle; GDVN, gas-focused dynamic virtual nozzle; GI, crystalline glucose isomerase; GPCRs, G protein-coupled receptors; GV, *Cydia* pomonella granulovirus; HA, hyaluronic acid; HARE, hit and return; HEC, hydroxyethyl cellulose; HVE, high viscosity extrusion; LCLS, linear accelerator coherent light source; LCP, lipid cubic phase; MESH, microfluidic electrokinetic sample holder; NaCMC, sodium carboxymethyl cellulose; PAM, polyacrylamide; PEO, poly(ethylene oxide); SFX, serial femtosecond crystallography; SMX, serial millisecond crystallography; SR, synchrotron radiation; SX, serial crystallography; TbCatB, *Trypanosoma* brucei procathepsin B; XFEL, X-ray free electron lasers; XRD, X-ray diffraction.

far-reaching influence. In particular, the practical application of the X-ray free electron lasers (XFEL) in determination of protein structure [3–7] has become a landmark event in this field, announcing the arrival of a new era.

The structure determination of biomacromolecules and their complexes is a very important part of structural biology. The structural information of biomacromolecules and their complexes is very fundamental for understanding the nature of life [8–10]. Therefore, it is of great scientific significance and practical value to study the structure and function of biomacromolecules and their complexes, such as enzymes.

At present, XRD, NMR, and cryoelectron microscopy are the main approaches to obtain the structure information of biomacromolecules and their complexes at the atomic scale. Each of the three approaches has its own advantages and is very important in the analysis of macromolecular structure. Among these techniques, XRD is still the most widely used for structural determination [11,12]. According to the statistics in PDB database (http://www.rcsb.org/stats/summary), more than 90% of the total protein structures were obtained by XRD. In the past, a successful diffraction experiment usually required the crystal to be large enough [13]. With the progress in X-ray light sources, X-ray detectors, and data processing technology, the size of crystals in diffraction experiments has been decreasing [14]. For example, the synchrotron radiation (SR) source can use micron-sized (as small as 10 μm) crystals for diffraction experiments, and the XFEL can perform diffraction experiments using crystals with a size of nanometers [15]. In general, for the same sample, the stronger the light source, the better the experimental results. However, a stronger light source will lead to an increase in the X-ray absorption dose, resulting in serious radiation damage [16]. Currently, the radiation damage of the crystal is usually reduced by flash-freezing the crystal in XRD experiments [17,18]. However, flash-freezing crystals can lead to some other problems [19,20]. These problems typically include: (a) More procedures are necessary to screen cryoprotectants to avoid the damaging of crystals during flash-freezing. (b) Flash-freezing of crystals can cause them to deteriorate, resulting in non-diffracting crystals. (c) Some proteins undergo structural changes during flash-freezing, which is not desirable for correct structure determination. (d) Low-temperature diffraction may lead to a significant increase in mosaicity [17,18,21]. (e) Though different conformational states can be trapped by flash-freezing to capture different conformational dynamics, it will be easier to study structural dynamics using crystals at room temperature.

The emergence of SFX provides an alternative for small protein crystal suspensions that do not require flash-freezing. The advantages of this technique are apparent: it not only avoids the procedures of flash-freezing crystals but also provides the structure information of proteins at physiological or near-physiological state. Besides, SFX can use micron and even submicron samples to determine the structure of proteins. During the SFX experiment, crystals are continuously delivered to the X-ray beam, then the diffraction data of thousands of single crystals are obtained and merged for solving the molecular structure [22]. Theoretically, this technique can achieve 'diffraction before destruction' [23]. In addition, it also enables time-resolved structural analysis, which provides an alternative to carry out studies in the structural dynamics of biological macromolecules [24–27].

SFX pioneered a new era in the structural analysis of the biological macromolecules. Moreover, the concept and method of SFX have been successfully validated on SR. The serial crystallography (SX) experiment performed on the SR is called serial millisecond crystallography (SMX). The emergence of SMX has made SFX expanded to SX that can additionally employ SR as the light source [28–32]. SMX inherits many advantages of SFX. For example, the complete structure of a molecule can be obtained by merging the data of multiple crystals; the size of the crystals used can be on the order of a few microns, which is of great value for proteins that are difficult to grow into large-size crystals; and the diffraction experiments can be carried out at room temperature, which is of particular importance for protein crystals that are not suitable to be frozen.

As a booming technology, the development of SX is affected by various aspects including hardware systems, data processing software, and the standardization of experimental technologies. The development of hardware systems is the basis of SX experiments which mainly includes sample delivery system, X-ray light source, and X-ray detector. The progress of SX experiments strongly relies on the development of X-ray light sources and X-ray detectors. In addition to these two hardware systems, the sample delivery system is crucial hardware for SX experiments. To advance the progress of SX, a series of sample delivery systems have been developed internationally. This review is focused mainly on existing sample delivery systems, summarizing their development and proposing their future prospectives.

Instrumentation of sample delivery systems

The major hardware equipment to complete SX data collection includes the diffraction light source (X-ray source), sample delivery system, and high-sensitivity detector (X-ray detector), as shown in Fig. 1. Sample delivery has always been a major focus for researchers since the advent of SX. A variety of sample delivery systems have already been developed for SX on XFEL facility [33,34], some of which have also been proven to be suitable for SR facility [35–37]. Sample delivery devices provide an SX experiment with samples moving through the X-ray beam. An ideal sample delivery system would enable fast data collection, with as low as possible sample consumption, data collection time, and diffraction background. It would be compatible with both XFELs and SR sources and would enable time-resolved measurements.

Existing sample delivery systems can be divided into two major categories, one with the process of crystal migration and the other without crystal migration relative to the delivery device. We name the first type as the moving target system and the second as the fixed-target system. For reference, we list the information about sample delivery systems summarized in this review in Table 1, including flow rate, sample delivery speed, sample consumption, crystal sizes, operating platforms (SR/XFEL), and examples of biological sample examined in SX experiments.

Moving target system

Moving target systems refer to a number of delivery systems containing a crystal migration process, which forms a stream of samples that can be continuously hit by X-rays. The sample stream is usually formed by using X-ray transparent glass capillary, nozzle jetting, etc. Typical moving target systems include the gas-focused dynamic virtual nozzle (GDVN), high-viscosity extrusion (HVE) injector, microfluidic electrokinetic sample holder (MESH), etc.

Gas-focused dynamic virtual nozzle

Gas-focused dynamic virtual nozzle is the first sample delivery system to deliver crystals in a flowing liquid suspension across an XFEL beam at the linear accelerator coherent light source (LCLS) [38]. Currently, the GDVN is one of the most commonly used technologies for sample delivery, and it is widely used in time-resolved studies such as mix and injections experiments [39,40]. GDVN is usually composed of two capillaries; one capillary is centered in the interior of the other, thus forming two channels. When the liquid is ejected, a high-pressure gas flow coaxial with the sample flow is ejected from the external chamber to form a 'virtual nozzle'. The 'virtual nozzle' focuses the jet down from a 50-μm capillary to a few microns jet so that the background can be reduced effectively, and at the same time, it can reduce the vacuum evaporation effect [22,41,42]. In addition, the sheath gas keeps the jet from freezing so that the detector does not get damaged by high-intensity ice diffraction. In order to keep the sample focused into a microjet during GDVN operation, a relatively fast liquid flow rate is required, typically at a speed of 10–20 $m \cdot s^{-1}$ [43]. After the European XFEL facility was put into operation, the requirements for a sample delivery system capable of matching its MHz pulse rate were put forward. Several SX experiments based on GDVN technology have been successfully carried out at the European XFEL facility [44–46]. Research shows that it is feasible to achieve SX sample delivery at MHz pulses by

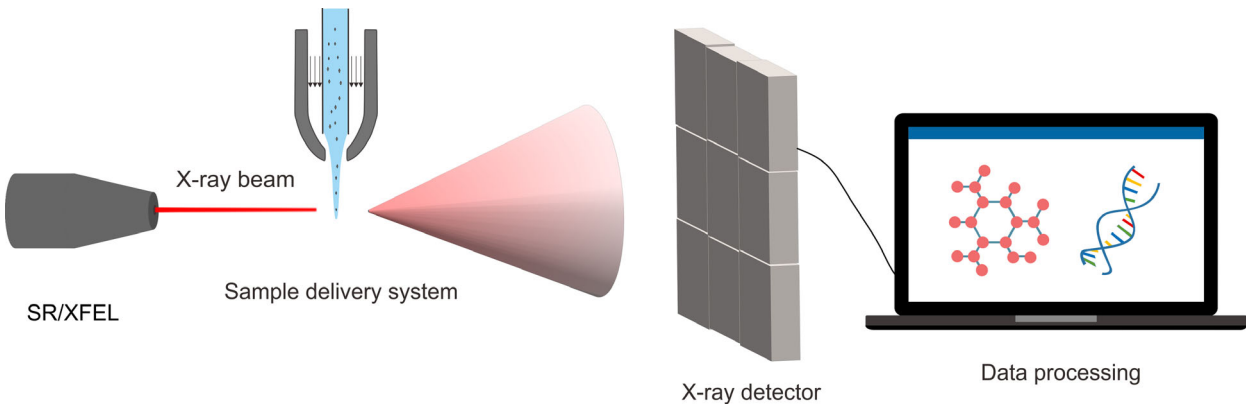

Fig. 1. Schematic representation of SX experiments, including X-ray source, sample delivery system, X-ray detector, and data processing.

Table 1. Sample delivery system and relevant information for SX experiments.

Systems	Technique name	Flow rate	Delivery speed	Sample consumption	Crystal sizes	SR/XFEL	Examples of biological samples
Moving target system	GDVN	~ 10–20 $\mu L \cdot min^{-1}$	~ 10–20 $m \cdot s^{-1}$	Dozens of milligrams or more	~ 5 μm	XFEL	Lysozyme; β-lactamase; RNA polymerase II; CcO; photosystem I; photosystem II;
	Capillary	2.5 $\mu L \cdot min^{-1}$	5×10^{-3} $m \cdot s^{-1}$	250 mg	Smaller than the inner diameter of the capillary	SR	Lysozyme
	HVE injector	~ 0.001–0.3 $\mu L \cdot min^{-1}$	Up to several millimeters per second	< 1 mg	~ 1–30 μm	SR and XFEL	Lysozyme; bR; CA II; thermolysin; crystalline GI; phycocyanin; thaumatin; proteinase K; sindbis virus
	MESH	~ 1–3 $\mu L \cdot min^{-1}$	Adjusted by applied voltage	Hundreds of micrograms	Up to 40 μm	XFEL	Thermolysin; 30S ribosomal subunit; photosystem II
	Aerosol injector	~ 2.7–3.5 $\mu L \cdot min^{-1}$	A few hundred meters per second	–[a]	Nanoscale	XFEL	GV
	ADE	Drop on demand	N/A	Hundreds of micrograms	~ 5–400 μm	XFEL	Thermolysin; lysozyme; photosystem II; phytochrome photoreceptor; RNR
Fixed-target system	Nylon loop	Defined by steps	N/A	Dozens of large crystals	> 50 μm	SR and XFEL	TbCatB; CcO; CuNiR; CpI hydrogenase
	Microfluidic chip	Defined by motors	N/A	Several micrograms	Depending on the chip	SR and XFEL	Lysozyme; BeV2; CPV18; hexagonal (P6) myoglobin; thaumatin; crystalline GI; thioredoxin
	Conveyor belt	Defined by motors	N/A	Hundreds of micrograms	Depending on the nozzles or syringes	SR and XFEL	Photosystem II; phytochrome photoreceptor

[a] No successful example yet.

designing and manufacturing nozzles that generate a small-diameter and high-speed jet [47].

The traditional GDVN is manufactured by manual flame polishing, limiting the resolution, repeatability, and yield of nozzles. To address this issue, technologies such as microfluidic chips based on soft lithography [48,49], ceramic microinjection molding [43], and three-dimensional printing based on two-photon polymerization [50] have been applied in nozzle manufacturing.

The high sample consumption of GDVN technology limits its application in the structural analysis of some difficultly crystallized proteins and valuable proteins. In 2017, Oberthuer [51] proposed the double-flow focusing nozzle (DFFN), and the structure of RNA polymerase II was obtained for the first time at room temperature using the DFFN device. The internal liquid flow of the DFFN is focused by a coaxially faster external liquid flow, and the external liquid flow is focused by a gas. In Fig. 2A, we show the constructions of the GDVN and DFFN. Compared with the GDVN, the DFFN significantly reduces the sample consumption because the liquid flow of the DFFN is mainly formed by the sheath fluid.

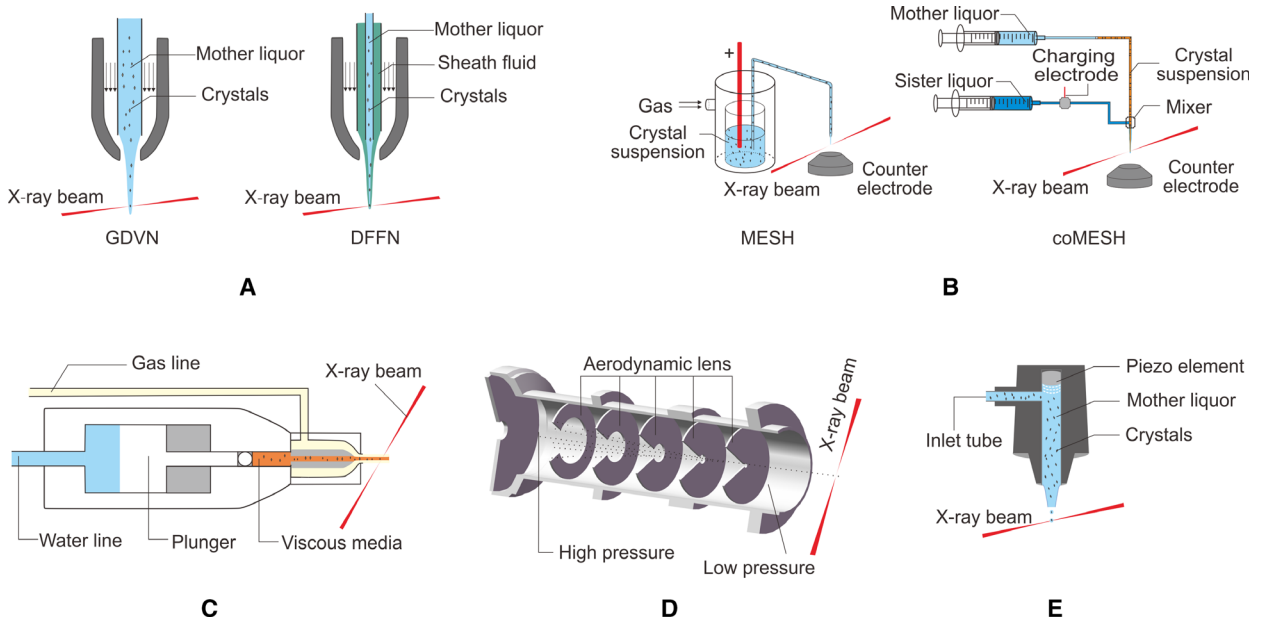

Fig. 2. Schematic representation of moving target system. (A) Diagram of the GDVN and DFFN system. (B) Diagram of MESH and CoMESH system. (C) Diagram of an HVE injector. (D) Diagrammatic representation of the cross-section of the aerodynamic lens. (E) Diagram of the nozzle of ADE technology.

Capillary delivery

The capillary delivery technique enables sample delivery by pushing the sample liquor in the capillary through an injection pump. In 2014, Chapman's team [30] carried out the proof-of-principle measurement. They analyzed the structure of lysozyme 2.1 Å at room temperature for the first time through the capillary delivery technology on SR, which verified the feasibility of synchrotron SX. A glass capillary, having an inner diameter of 100 μm and a wall thickness of 10 μm, was used in their experiments. The experimental process was run at a flow rate of 5 μm·ms^{-1} (2.5 μL·min^{-1}), which effectively reduced sample consumption, but the slower sample delivery speed increased the run time of the crystal in the pipeline, which brought serious crystal settlement. Therefore, during the measurement, the capillary was simultaneously scanned to avoid accumulation of the sample on the wall of the capillary. In this device, the influence of diffraction background comes from the solution in the pipeline and the material of capillary. Selecting a capillary with a smaller diameter and lower diffraction background can make a significant contribution to reducing the diffraction background.

Recently, another device belonged to capillary delivery has been reported. In their research, a metal-polyimide microfluidic flow-focusing device was designed and manufactured. This research achieved SMX data collection in the microfluidic flow-focusing device, and it has the advantages of low sample consumption and short time consumption [52]. Polyimide (Kapton) is an ideal material for delivery devices because it is widely used in X-ray scattering and diffraction experiments. To use the Kapton as a material for capillary delivery devices has the advantage of reduced cost and background scattering.

High-viscosity extrusion (HVE) injector

High-viscosity-extrusion is also known as lipid cubic phase (LCP) extrusion. This is a method developed from the liquid jet technique. Figure 2C shows a diagram of an HVE injector. The constructions of the HVE injector and GDVN nozzle are similar. Since the medium used in an HVE injector is relatively viscous, the sample flow rate is slow when extruded (0.001–0.3 μL·min^{-1}); therefore, the utilization of crystals can be significantly increased, and the sample consumption can be reduced effectively [53–55].

Initially, LCP technology was mainly used for membrane protein crystals [56]. The progress of structure research in membrane proteins is far behind that of soluble proteins because membrane proteins are not easily crystallized and they are relatively unstable once they are separated from their natural lipid bilayer

environment [57]. The development of membrane protein structure analysis benefits from the LCP crystallization method. In 1996, Landau [58] first crystallized the bacterial rhodopsin protein by the LCP technique. Subsequently, a variety of membrane protein structures, including G protein-coupled receptors (GPCRs), was obtained by LCP technology [59–65]. GPCRs mediate signaling pathways and participate in the regulation of a variety of physiological processes and are important drug targets.

Recently, the successful application of LCP-SFX [57,66–68] in the structure determination of membrane proteins has shown that the structural analysis of membrane proteins can be achieved with tiny crystals. This step is of great importance to the structure determination of membrane proteins, which typically form small-sized crystals in the LCP. In LCP-SFX technology, the LCP acts as a medium both for the growth of membrane protein microcrystals and for the delivery of membrane protein microcrystals. It has been shown that viscous injectors are unrestricted by the medium, and the range of media has been successfully extended to grease-matrix [69], agarose [70,71], vaseline [36], poly(ethylene oxide) (PEO) [72], hyaluronic acid (HA) [73], polyacrylamide (PAM) [74], and hydrogels [hydroxyethyl cellulose (HEC), sodium carboxymethyl cellulose, and Pluronic F-127] [75,76], etc.

Lipid cubic phase-SFX technology is also suitable for soluble proteins. In 2015, Fromme [77] successfully used the LCP as a medium for soluble proteins to collect high-quality LCP-SFX datasets of lysozyme and phycocyanin, reducing the consumption of each protein to < 0.1 mg. In 2018, the structural data of carbonic anhydrase II (CA II) crystallites were collected by LCP-SFX technology, which laid the foundation for the time-resolved study of CA II catalysis by SX experiment [78]. The serial diffraction experiment can be achieved by the same method when soluble protein crystals are dispersed in other relatively viscous media. In 2015, Conrad [70] explored and developed a novel delivery medium based on agarose. The agarose medium is available for both soluble proteins and membrane proteins. Compared with the LCP and other viscous delivery matrices, the agarose delivery can produce a low X-ray scattering background. In 2016, Sugahara [73] reported the water-based HA matrix crystal carrier which is suitable for oil-sensitive protein crystals, and it was successfully used for proteinase K and lysozyme. The HA matrix can achieve low sample consumption and significantly reduce background scattering. However, because of the strong adhesion of HA, the nozzle is easily clogged. In 2017, Sugahara [75] used an HEC matrix as the crystal carrier to obtain structures of soluble proteins at a resolution beyond 1.8 Å at room temperature. The HEC carrier can produce a stable and small-diameter sample flow, and it is helpful to reduce sample consumption and background scatter. More recently, the application of PAM in sample delivery as a viscous matrix has been reported. The outstanding advantage of PAM as a sample delivery matrix is that it will not have a binding reaction with protein samples [74].

Currently, the HVE injector can perform on both SR and XFEL facilities. In 2015, Nogly *et al.* [79] implemented an LCP-SMX experiment on the ESRF microfocus beamline and obtained the structure of the light-driven proton pump bacteriorhodopsin (bR) with a resolution of 2.4 Å. The authors also carried out LCP-SFX experiments on a LCLS using the same sample [80]. In 2017, Martin-Garcia [72] carried out an SMX experiment based on HVE technology at the Advanced Photon Source. In this research, crystals with a size of 5–20 μm suspended in the LCP or PEO were delivered to the SR beam by a high-viscosity injector. The successful validation of LCP-SMX extends LCP-SFX technology to LCP-SX technology, which will promote progress in the structural analysis of membrane proteins as well as soluble proteins.

Microfluidic electrokinetic sample holder

The MESH is also known as an electrospin injector. The MESH uses a high-voltage electric field to focus the liquid flow for sample delivery and primarily works in SFX experiments, which usually perform under a vacuum environment. This technology reduces sample consumption by adding an additive with moderate viscosity to the sample suspension.

In 2012, Sierra [81] used a MESH device for nanoflow electrospinning under a vacuum environment. To reduce sample consumption, glycerol was added to the sample suspension and successfully achieved a low sample consumption of 0.14–3.1 $\mu L \cdot min^{-1}$; however, its background interference was high. In addition, since the experiment was performed under vacuum conditions, the evaporation of the sample liquid was rapid. The rapid evaporation of the sample liquid led to the dehydration of crystals, and the evaporation of the sample liquid absorbed heat from its surroundings causing the sample to freeze. The evaporation of the sample liquid also resulted in the precipitation of the solvent, which seriously affected the sample ejection. Then, Sierra [82] developed the concentric-flow electrokinetic injector (CoMESH) to solve these problems. In Fig. 2B, we show diagrams of the MESH and CoMESH. Compared with the MESH, the CoMESH

uses a concentric capillary design. The inner capillary introduces crystals suspended in the mother liquor to the XFEL beam. The sheath flow in the outer capillary protects the sample from vacuum-induced evaporation, preventing the sample from dehydrating and freezing as it is introduced into the vacuum chamber while reducing the background interference. Sierra used CoMESH to collect the first complete data of the 30S subunit bound to the antibiotic paromomycin at ambient temperature [82]. This achievement is of great importance for the structural-based drug design of a new generation of antibiotics against bacterial ribosomes.

Microfluidic electrokinetic sample holder technology typically maintains a flow rate of 1–3 $\mu L \cdot min^{-1}$, which allows sample consumption of 10–100 times lower than that of the aerosol injectors and GDVN. The MESH is an ideal sample delivery technology for SX experiments, whether it is a simple protein or a complex membrane protein. In the future, the prospect of developing MESH devices for sample delivery used in both SR and XFEL facilities is attractive.

Aerosol injector

The aerosol injector is a device utilizing a nozzle to jet aerosol particles under high pressure at a high velocity, including electrically driven aerosol injectors and gas driven aerosol injectors [83]. Atomized droplets containing sample generated by aerosol injectors pass through a series of separators, apertures, and graded pumps, eventually entering the vacuum environment to deliver the sample to the X-ray beam. The aerosol injector reduces the amount of liquid around the sample during sample delivery, thereby the background scanning can be reduced effectively. However, the disadvantage of aerosol injectors is the low hit rate, which is a feature that needs to be optimized [84].

A typical aerosol injector is atomized by a GDVN and then focused by an aerodynamic lens and delivered to an XFEL beam [85–87]. An aerodynamic lens is also known as a coaxial lens and consists of a series of concentric axis-symmetric apertures (see Fig. 2D). The aerodynamic lens migrates the particles toward the central streamline by adjusting the interaction between the inertial forces of the particles and the gas resistance. The aerodynamic lens can be designed by formulas and software for producing different diameters of particles. The aerosol injector can emit particles at a high speed, and it is the only technology currently developed in which the sample flow rate can be matched with the European XFEL facility [88].

In 2008, Bogan [89] demonstrated the diffraction imaging of a nanoscale sample in free flight by aerodynamic lens for the first time, and laid the foundation for single-particle coherent diffraction imaging (SPI) of biomolecules. SPI benefits from the superbright X-ray pulses generated by an XFEL, and SPI technology can image nanoscale samples effectively without the need for crystallization [90]. As a successful technique for SPI research, aerosol injector has been successfully used in the study of viruses [86–88,91], soot [92], cells [93], cell components [94], and so on.

Preliminary studies have suggested that the aerosol injector is not suitable for biological macromolecular crystals, which need to be kept in a liquid or semi-liquid medium. In 2018, Chapman and colleagues conducted SFX studies on natural *Cydia pomonella* granulovirus (GV) nanocrystals by an aerosol injector. The author also proposed that when using other protein crystals that are not stable enough in pure water, a suitable strategy should be adopted to control the relative humidity of the crystals [95]. These results also indicate that the aerosol injector is a potential technology for delivering crystal samples into X-ray beams [96].

Acoustic droplet ejection

Acoustic droplet ejection (ADE) uses sound pulses to deliver samples from a source location to a variable destination through a short air column, as shown in Fig. 2E. ADE can jet nanoliter or picoliter droplets with high positional precision and repeatability. The size and velocity of the droplet are governed by the frequency and amplitude of the emitted sound.

ADE technology was originally used for protein crystal growth, improvements in crystal quality, high-throughput screening, dose–response experiments, and so on. In 2015, Wu [97] researched the application of ADE technology in crystallization experiments at the low-nanoliter scale. The researcher also described an automation system that combines an acoustic liquid processor with a robot arm and other related auxiliary devices to achieve unattended high-throughput crystallization experiments. In 2016, Ericson [98] described a method for detecting protein crystals and monitoring crystal growth using the ADE system. Currently, the ADE system can detect crystals < 50 μm in size, and experimentalists expect using this system to detect and monitor the growth of 3-μm single crystals.

Now, ADE technology is gradually being developed for sample delivery. ADE delivery systems use focused acoustic waves to jet droplets containing crystals into an X-ray beam for diffraction experiments and data collection. In 2016, Roessler [99] proposed two kinds

of ADE systems for sample delivery, one is a positive system and the other is an inverted system. Both of them enabled drop-on-demand with a high hit rate. The inverted system provided repeatable size and velocity of the droplet and effectively counteracted the settlement of crystals. In 2017, Fuller [100] combined ADE with a Kapton conveyor belt achieving drop-on-demand sample delivery. The samples were deposited on the Kapton belt by an acoustic injector and then delivered to the X-ray beam through the Kapton conveyor belt. This system is not only suitable for the structural determination of proteins but also for the in situ determination of many enzymatic intermediates [101].

Acoustic droplet ejection technology can be used to deliver large-size samples without the clogging problem characteristic of GDVN technology. Successful application of the ADE delivery system at the XFEL facility has been verified. Since the ADE delivery system enables drop-on-demand, the development of an ADE system for an SR facility is achievable by adjusting the ejection frequency of the ADE system.

Fixed-target system

Fixed-target systems refer to those without crystal migration during diffraction. In other words, the crystals are fixed in a sample holder. Serial crystallographic diffraction is realized by moving the sample holder so that different crystals can be hit. When using the fixed target for a diffraction experiment, a prescan is often performed to determine the position of the crystals, and later, the entire fixed target is moved to perform the diffraction experiment right on the crystals. In 2016, Oghbaey [102] used a fixed target in combination with spectroscopic mapping providing a versatile and efficient system that achieved a hit rate approaching 100%. Compared with the moving target systems, the fixed-target systems can usually reduce the sample consumption. Typical fixed-target systems include nylon loops, microfluidic chips, and so on.

Nylon loop

Sample delivery by nylon loops is achieved by suspending single or multiple crystals in a nylon loop and then performing a click-and-shoot, raster, or helical scan of the crystals for data collection. Unlike other techniques, data collection through a nylon loop allows multiple-exposure data for the same crystal, and the experiment can be conducted at both cryogenic and ambient temperatures [103].

Figure 3A shows a diagram of an experimental setup for helical data collection with a nylon loop. Different horizontal, vertical, and rotational steps can be set according to the experimental needs. The helical data collection is very suitable for long crystals. In 2014, Hirata [104] collected the structural data of cytochrome *c* oxidase (CcO) with up to 1.9 Å resolution through the helical scanning method at the SPring-8 angstrom compact free-electron laser facility. This method is not only suitable for XFELs but also compatible with many existing synchrotron beamlines. In 2014, Gati [28] obtained a complete dataset of *Trypanosoma brucei* procathepsin B (TbCatB) at a 3 Å resolution by serial SR crystallography. In their study,

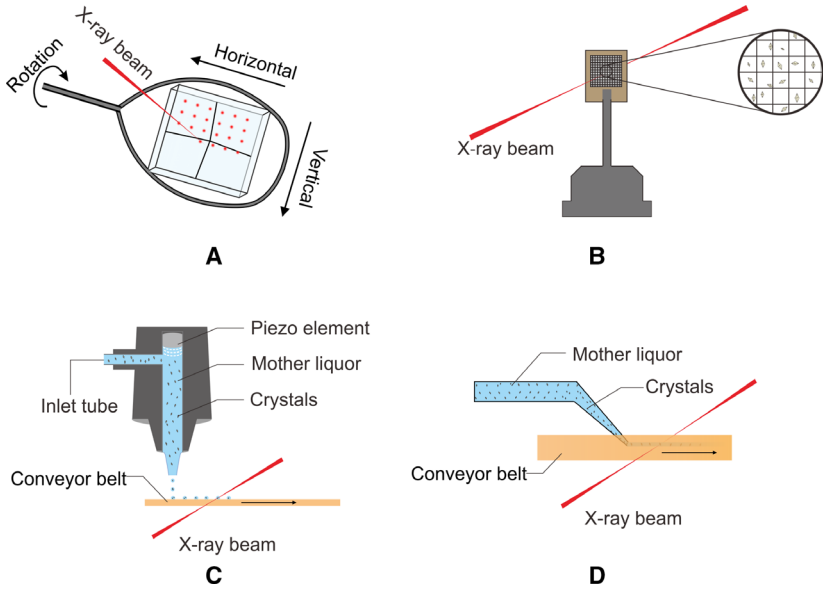

Fig. 3. Schematic representation of fixed-target systems. (A) Diagram of an experimental setup for helical data collection of nylon loop [104]. (B) Diagram of a microfluidic chip device. (C) Conveyor belt combined with ADE for sample delivery. (D) Conveyor belt combined with syringes for sample delivery.

the TbCatB microcrystalline suspension grown *in vivo* was mounted on a nylon loop, and the loop was spirally scanned. Recently, the X-ray damage-free structure of copper nitrite reductase (CuNiR) at a 1.6 Å resolution was obtained by the helical scanning of large crystals in nylon loops [105].

Microfluidic chip

Microfluidic chips used in SX experiments are usually composed of thin films or silicon wafers with micropores. The SX is realized by loading single microcrystals in the micropores and then conducting raster scanning. Figure 3B shows an example of a typical microfluidic chip.

In 2014, Hunter [106] successfully verified the sample delivery strategy of a fixed-target device with low sample consumption by loading protein microcrystals onto an ultra-thin silicon nitride membrane. In 2015, Coquelle [107] designed a sandwich-like silicon nitride device, and lysozyme crystals in two silicon nitride wafers were presented to the X-ray beam for the diffraction experiment, obtaining a high-resolution structure of lysozyme up to 1.7 Å. In 2015, Roedig [108] developed a micropatterned silicon chip as the sample holder to load up to thousands of crystals. The micropatterned silicon chip can fix crystals suspended in mother liquor effectively. Additionally, the chip allows removing the mother liquor efficiently. Therefore, the background interference can be reduced. In addition, the micropatterned silicon chip is appropriate for a wide size range of crystals from very small to medium, but the crystals are prone to dehydration during the longer data collection. To solve this problem, Roedig [109] suggested exposing crystals to a humidified air or helium chamber during the experiment. The strategy of sealing chips with a polyimide film or graphene can also protect crystals from dehydration [110,111]. In 2017, Roedig [112] combined the micropatterned silicon chip with a high-speed roadrunner goniometer for sample delivery in an SX experiment, and for the first time, they obtained the complete structure of bovine enterovirus 2 (BeV2) at the atomic level through XRD methods. In their research, a micropatterned silicon chip containing thousands of pores was used to hold samples, and then the X-ray beam scanned the chip line by line. This technology achieved a high hit rate in the diffraction experiment, and complete dataset of BeV2 was obtained within 14 min. Moreover, only 0.23 nL of the sample was consumed. The authors also used the method to collect the dataset of cytoplasmic polyhedrosis virus type 18 polyhedrin (CPV18), and the structure of the CPV18 crystals was solved with only ~ 4 μg of protein. Such a requirement is of great significance for the structural analysis of some samples that are difficult to obtain in large quantities. More importantly, the success of this research opened up a new approach for the structural analysis of viruses, and it has been much helpful to the structural analysis of more viruses. For microfluidic chip technology, sample loading is a challenging process. In 2018, a sheet-on-sheet sandwich device was designed to address this challenge and has proven effective [113]. The sheet-on-sheet sandwich is made up of two nonmicromachined Mylar films and crystal samples between them.

Recently, the microfluidic chip technology has been applied to dynamic study in an SX experiment; Schulz [114] designed the 'hit and return' (HARE) method of serial synchronous radiation crystallography for time-resolution research based on the silicon wafer technology of a fixed target, realizing dynamic study with a time resolution from milliseconds to seconds or even longer. The 'HARE' method expands the fixed-target technology from sample delivery technology to time-resolution research technology. Moreover, the approach's high flexibility in time resolution makes it very ideal for the detection of multiple biological reactions.

Microgrids or micromeshes, similar to microfluidic chips, have also been developed for sample delivery. In 2014, Cohen [103] investigated the feasibility of a grid as a data collection strategy for SX experiments, and then Cohen *et al.* undertook an SX experiment with the grid [115]. In their study, hexagonal (P6) myoglobin crystals were loaded into the grid manually, and finally, a complete data set at 1.36 Å was obtained from 932 crystals in 32 grids. The researchers also described a technology for growing crystals in the grid incubation chamber and loading crystals into grids by liquid-handling robots. In 2017, a sample extractor was designed for sample delivery. This device captures crystals from their mother liquor using a mesh or a film as the substrate, and then the substrate with sample are encapsulated in a small vial. The vial has openings on both sides, which are covered with a thin X-ray transparent film to ensure the X-rays pass through, and reduces dehydration of the crystals during diffraction [116].

Transferring crystals to microfluidic chips, grids, or other sample delivery systems increases the risk of damage and loss of crystals, but this problem can be avoided effectively by combining sample delivery systems with crystal growth devices [117]. This technique of directly collecting the crystal diffraction data in the growing environment without transferring crystals is often termed as in situ diffraction technology. In 2018,

Gicquel [118] proposed a microfluidic device with a soft lithography-patterned epoxy resin as filler and a polyimide foil as a window, revealing that the microfluidic device is suitable for in situ protein crystallization and diffraction data collection. Other in situ devices, such as the crystal-on-crystal chip, have been developed for more in situ research [119]. In situ diffraction technology can not only avoid the damage and loss of crystals but also obtain the molecular structure in the growth environment of crystals. The development of in situ diffraction technology deserves the attention of researchers.

Conveyor belt system

Conveyor belt systems are commonly used as part of a sample delivery system to connect with other devices, such as nozzles or syringes (Fig. 3C,D), for sample delivery. It has been proven feasible to deposit a crystal suspension on the conveyor belt by spray or injection. Kapton film is a preferred material for conveyor belts due to its excellent X-ray transmission properties. In 2017, Chapman *et al.* [120] combined a new Kapton belt drive with a microfluidic mixer to determine the structure of the chitosan-lysozyme binding with a mixing time from 2 to 50 s, indicating that serial SR crystallography is available for studying the mixing and diffusion of ligand binding. In their study, the suspension containing the protein crystals was mixed with the ligand and then deposited onto the Kapton belt to achieve sample delivery and time-resolved studies with SX by continuous pulling of the Kapton belt. The new combination of Kapton belt driver and microfluidic mixer is expected to be used in the study of structural enzymology. The conveyor belt has also been combined with ADE equipment for sample delivery and time-resolved research [100,101].

Practical considerations for more efficient sample delivery

Antisettling of crystals

For liquid flow technologies such as liquid jet technology, the settlement of crystals caused by gravity is inevitable. In 2012, Lomb [121] developed an antisettling sample delivery instrument based on a rotary syringe pump, which has been successfully used for different protein crystals. The technique can effectively resist the settlement of crystals smaller than 20 μm in size. Until recently, this method was still a commonly used antisettling measure [44]. In capillary sample delivery technology studies, the strategy to avoid crystal accumulation on the tube inner wall by scanning the capillary during sample delivery has also proven effective [30]. In 2017, Beyerlein [120] prevented crystal settling by connecting a sample reservoir containing a microcrystalline suspension to the motor and programming the motor to rotate 180° back and forth. The above measures are based on the principle of mechanical motion to achieve antisettling. In the development of new and more efficient sample delivery technologies, finding new solutions that are simpler and easier to use to avoid crystal settling remains of great importance.

Delivery speed

X-ray free electron lasers and SR sources have different requirements for sample delivery speeds, and XFEL requires faster speeds. XFEL devices with megahertz repetition rates place high demands on sample delivery speeds. The sample delivery rate required for a SR source is very slow compared to that of an XFEL. Developing a sample delivery technology that is compatible with both types of light sources presents significant challenges. In addition, the value of SX is reflected in its alternative methods for not only traditional crystallography but also the fields of structural dynamics and phase transitions, which have increasingly attracted researchers' attention in recent years. The sample delivery speed in SX should be matched with the light source on the one hand, and the application of the study to time resolution should be considered on the other hand. Therefore, it is worthwhile to further develop a sample delivery device that is adjustable in speed over a wider range.

In situ data collection

In situ diffraction data collection techniques have become a trend because sample transfer processes prior to sample data collection and during data collection can cause some loss of crystal in mass and quality, reducing crystal availability. It is of great significance to seek a completely in situ solution from crystal growth to diffraction data collection for the consumption of experimental samples and the physiological state of biological samples.

Concluding remarks

Serial crystallography has demonstrated advantages that were not easy to achieve in the past. For SX, the size of crystals is no longer a limiting factor, and the radiation damage can be avoided by 'diffraction before destruction'. Furthermore, the unique merits of SX,

such as spatial and temporal structure studies and room-temperature diffraction, have greatly promoted the development of structural biology. The development of SX has also inspired progress in X-ray light sources and X-ray detectors.

In this article, we reviewed the latest progress of sample delivery systems for SX. As an indispensable part of SX, sample delivery has become a research focus in many laboratories. As long as fresh crystals can be continuously provided for diffraction, a complete dataset can be obtained by merging these diffraction data. However, existing sample delivery systems still need to be further optimized with careful consideration to the sample consumption, cost, and compatibility of samples and equipment. Developing a simple, efficient, and compatible sample delivery system remains a major trend. In addition, the time needed for obtaining the structure of biomolecules by SX technology still needs to be further shortened; it is hoped that the structure of biomolecules can eventually be obtained in a few minutes or even shorter by SX technology. Moreover, the requirements (such as the cost) to the construction of SR and XFEL facilities may limit the popularity of SX experiments. Therefore, developing laboratory-level X-ray light sources may become a new direction.

Acknowledgements

This work was supported by the National Natural Science Foundation of China (Grant No. U1632126), 921 project of China (Grant No. 17430206), and the Peak Plan of Northwestern Polytechnical University (Grant No. 17GH020843).

Conflicts of interest

The authors declare no conflict of interest.

Author contributions

FZZ, JHH, and DCY planned the content of the article; FZZ and DCY wrote the text; FZZ drew the figures; BZ and EKY edited the figures; DCY, JHH, BS, and ZJW edited the article.

References

1 Ewald PP (1913) The theory of the interference of X-rays in crystals. *Phys Z* **14**, 465–472.
2 Bragg WL & Thomson JJ (1914) The diffraction of short electromagnetic waves by a crystal. *P Camb Philos Soc* **17**, 43–57.
3 Loh ND (2014) A minimal view of single-particle imaging with X-ray lasers. *Philos Trans R Soc Lond B Biol Sci* **369**, 20130328.
4 Redecke L, Nass K, DePonte DP, White TA, Rehders D, Barty A, Stellato F, Liang M, Barends TR, Boutet S *et al.* (2013) Natively inhibited *Trypanosoma brucei* cathepsin B structure determined by using an X-ray laser. *Science* **339**, 227–230.
5 Schlichting I & Miao J (2012) Emerging opportunities in structural biology with X-ray free-electron lasers. *Curr Opin Struct Biol* **22**, 613–626.
6 Koopmann R, Cupelli K, Redecke L, Nass K, Deponte DP, White TA, Stellato F, Rehders D, Liang M, Andreasson J *et al.* (2012) *In vivo* protein crystallization opens new routes in structural biology. *Nat Methods* **9**, 259–262.
7 Boutet S, Lomb L, Williams GJ, Barends TR, Aquila A, Doak RB, Weierstall U, DePonte DP, Steinbrener J, Shoeman RL *et al.* (2012) High-resolution protein structure determination by serial femtosecond crystallography. *Science* **337**, 362–364.
8 Chen CC, Han X, Ko TP, Liu WD & Guo RT (2018) Structural studies reveal the molecular mechanism of PETase. *Febs J* **285**, 3717–3723.
9 Wilk P, Uehlein M, Piwowarczyk R, Dobbek H, Mueller U & Weiss MS (2018) Structural basis for prolidase deficiency disease mechanisms. *Febs J* **285**, 3422–3441.
10 Takeda K & Miki K (2017) Ultra-high-resolution structure and charge-density analysis of high-potential iron-sulfur protein. *Febs J* **284**, 2163–2166.
11 Chayen NE & Saridaki E (2008) Protein crystallization: from purified protein to diffraction-quality crystal. *Nat Methods* **5**, 147–153.
12 Yan EK, Zhao FZ, Zhang CY, Yang XZ, Shi M, He J, Liu YL, Liu Y, Hou H & YinD C (2018) Seeding protein crystallization with cross-linked protein crystals. *Cryst Growth Des* **18**, 1090–1100.
13 Nave C (1999) Matching X-ray source, optics and detectors to protein crystallography requirements. *Acta Crystallogr Sect D-Biol Crystallogr* **55**, 1663–1668.
14 Holton JM & Frankel KA (2010) The minimum crystal size needed for a complete diffraction data set. *Acta Crystallogr Sect D-Biol Crystallogr* **66**, 393–408.
15 Lee DB, Kim JM, Seok JH, Lee JH, Jo JD, Mun JY, Conrad C, Coe J, Nelson G, Hogue B *et al.* (2018) Supersaturation-controlled microcrystallization and visualization analysis for serial femtosecond crystallography. *Sci Rep* **8**, 2514.
16 Muench SP, Antonyuk SV & Hasnain SS (2019) The expanding toolkit for structural biology: synchrotrons, X-ray lasers and cryoEM. *IUCrJ* **6**, 167–177.
17 Warkentin M, Hopkins JB, Badeau R, Mulichak AM, Keefe LJ & Thorne RE (2013) Global radiation

damage: temperature dependence, time dependence and how to outrun it. *J Synchrot Radiat* **20**, 7–13.
18 Warkentin M, Atakisi H, Hopkins JB, Walko D & Thorne RE (2017) Lifetimes and spatio-temporal response of protein crystals in intense X-ray microbeams. *IUCrJ* **4**, 785–794.
19 Russi S, Gonzalez A, Kenner LR, Keedy DA, Fraser JS & van den Bedem H (2017) Conformational variation of proteins at room temperature is not dominated by radiation damage. *J Synchrot Radiat* **24**, 73–82.
20 Keedy DA, Hill ZB, Biel JT, Kang E, Rettenmaier TJ, Brandao-Neto J, Pearce NM, von Delft F, Wells JA & Fraser JS (2018) An expanded allosteric network in PTP1B by multitemperature crystallography, fragment screening, and covalent tethering. *eLife* **7**, e36307.
21 Southworth-Davies RJ, Medina MA, Carmichael I & Garman EF (2007) Observation of decreased radiation damage at higher dose rates in room temperature protein crystallography. *Structure* **15**, 1531–1541.
22 Chapman HN, Fromme P, Barty A, White TA, Kirian RA, Aquila A, Hunter MS, Schulz J, DePonte DP, Weierstall U *et al.* (2011) Femtosecond X-ray protein nanocrystallography. *Nature* **470**, 73–77.
23 Chapman HN, Caleman C & Timneanu N (2014) Diffraction before destruction. *Philos Trans R Soc B-Biol Sci* **369**, 20130313.
24 Li C, Schmidt K & Spence JC (2015) Data collection strategies for time-resolved X-ray free-electron laser diffraction, and 2-color methods. *Struct Dyn* **2**, 041714.
25 Tenboer J, Basu S, Zatsepin N, Pande K, Milathianaki D, Frank M, Hunter M, Boutet S, Williams GJ, Koglin JE *et al.* (2014) Time-resolved serial crystallography captures high-resolution intermediates of photoactive yellow protein. *Science* **346**, 1242–1246.
26 Stagno JR, Bhandari YR, Conrad CE, Liu Y & Wang YX (2017) Real-time crystallographic studies of the adenine riboswitch using an X-ray free-electron laser. *Febs J* **284**, 3374–3380.
27 Coquelle N, Sliwa M, Woodhouse J, Schiro G, Adam V, Aquila A, Barends TRM, Boutet S, Byrdin M, Carbajo S *et al.* (2018) Chromophore twisting in the excited state of a photoswitchable fluorescent protein captured by time-resolved serial femtosecond crystallography. *Nat Chem* **10**, 31–37.
28 Gati C, Bourenkov G, Klinge M, Rehders D, Stellato F, Oberthur D, Yefanov O, Sommer BP, Mogk S, Duszenko M *et al.* (2014) Serial crystallography on *in vivo* grown microcrystals using synchrotron radiation. *IUCrJ* **1**, 87–94.
29 Rossmann MG (2014) Serial crystallography using synchrotron radiation. *IUCrJ* **1**, 84–86.
30 Stellato F, Oberthur D, Liang MN, Bean R, Gati C, Yefanov O, Barty A, Burkhardt A, Fischer P, Galli L *et al.* (2014) Room-temperature macromolecular serial crystallography using synchrotron radiation. *IUCrJ* **1**, 204–212.
31 Hasegawa K, Yamashita K, Murai T, Nuemket N, Hirata K, Ueno G, Ago H, Nakatsu T, Kumasaka T & Yamamoto M (2017) Development of a dose-limiting data collection strategy for serial synchrotron rotation crystallography. *J Synchrotron Radiat* **24**, 29–41.
32 Standfuss J & Spence J (2017) Serial crystallography at synchrotrons and X-ray lasers. *IUCrJ* **4**, 100–101.
33 Chavas LM, Gumprecht L & Chapman HN (2015) Possibilities for serial femtosecond crystallography sample delivery at future light sources. *Struct Dyn* **2**, 041709.
34 Martiel I, Muller-Werkmeister HM & Cohen AE (2019) Strategies for sample delivery for femtosecond crystallography. *Acta Crystallogr Sect D-Struct Biol* **75**, 160–177.
35 Zarrine-Afsar A, Barends TRM, MullerC Fuchs MR, Lomb L, Schlichting I & Miller RJD (2012) Crystallography on a chip. *Acta Crystallogr Sect D-Biol Crystallogr* **68**, 321–323.
36 Botha S, Nass K, Barends TRM, Kabsch W, Latz B, Dworkowski F, Foucar L, Panepucci E, Wang MT, Shoeman RL *et al.* (2015) Room-temperature serial crystallography at synchrotron X-ray sources using slowly flowing free-standing high-viscosity microstreams. *Acta Crystallogr Sect D-Struct Biol* **71**, 387–397.
37 Grunbein ML & Kovacs GN (2019) Sample delivery for serial crystallography at free-electron lasers and synchrotrons. *Acta Crystallogr Sect D-Struct Biol* **75**, 178–191.
38 DePonte DP, Weierstall U, Schmidt K, Warner J, Starodub D, Spence JCH & Doak RB (2008) Gas dynamic virtual nozzle for generation of microscopic droplet streams. *J Phys D Appl Phys* **41**, 195505.
39 Stagno JR, Liu Y, Bhandari YR, Conrad CE, Panja S, Swain M, Fan L, Nelson G, Li C, Wendel DR *et al.* (2017) Structures of riboswitch RNA reaction states by mix-and-inject XFEL serial crystallography. *Nature* **541**, 242–246.
40 Ishigami I, Lewis-Ballester A, Echelmeier A, Brehm G, Zatsepin NA, Grant TD, Coe JD, Lisova S, Nelson G, Zhang SJ *et al.* (2019) Snapshot of an oxygen intermediate in the catalytic reaction of cytochrome c oxidase. *Proc Natl Acad Sci USA* **116**, 3572–3577.
41 Hutchison CDM, Cordon-Preciado V, Morgan RML, Nakane T, Ferreira J, Dorlhiac G, Sanchez-Gonzalez A, Johnson AS, Fitzpatrick A, Fare C *et al.* (2017) X-ray free electron laser determination of crystal structures of dark and light states of a reversibly photoswitching fluorescent protein at room temperature. *Int J Mol Sci* **18**, 1918.

42 Kupitz C, Basu S, Grotjohann I, Fromme R, Zatsepin NA, Rendek KN, Hunter MS, Shoeman RL, White TA, Wang DJ *et al.* (2014) Serial time-resolved crystallography of photosystem II using a femtosecond X-ray laser. *Nature* **513**, 261–265.
43 Beyerlein KR, Adriano L, Heymann M, Kirian R, Knoska J, Wilde F, Chapman HN & Bajt S (2015) Ceramic micro-injection molded nozzles for serial femtosecond crystallography sample delivery. *Rev Sci Instrum* **86**, 125104.
44 Grunbein ML, Bielecki J, Gorel A, Stricker M, Bean R, Cammarata M, Dorner K, Frohlich L, Hartmann E, Hauf S *et al.* (2018) Megahertz data collection from protein microcrystals at an X-ray free-electron laser. *Nat Commun* **9**, 3487.
45 Schulz J, Bielecki J, Doak RB, Dorner K, Graceffa R, Shoeman RL, Sikorski M, Thute P, Westphal D & Mancuso AP (2019) A versatile liquid-jet setup for the European XFEL. *J Synchrot Radiat* **26**, 339–345.
46 Wiedorn MO, Oberthur D, Bean R, Schubert R, Werner N, Abbey B, Aepfelbacher M, Adriano L, Allahgholi A, Al-Qudami N *et al.* (2018) Megahertz serial crystallography. *Nat Commun* **9**,4025.
47 Wiedorn MO, Awel S, Morgan AJ, Ayyer K, Gevorkov Y, Fleckenstein H, Roth N, Adriano L, Bean R, Beyerlein KR *et al.* (2018) Rapid sample delivery for megahertz serial crystallography at X-ray FELs. *IUCrJ* **5**, 574–584.
48 Trebbin M, Kruger K, DePonte D, Roth SV, Chapman HN & Forster S (2014) Microfluidic liquid jet system with compatibility for atmospheric and high-vacuum conditions. *Lab Chip* **14**, 1733–1745.
49 Doak RB, DePonte DP, Nelson G, Camacho-Alanis F, Ros A, Spence JCH & Weierstall U (2012) Microscopic linear liquid streams in vacuum: injection of solvated biological samples into X-ray free electron lasers. *Aip Conf Proc* **1501**, 1314–1323.
50 Nelson G, Kirian RA, Weierstall U, Zatsepin NA, Farago T, Baumbach T, Wilde F, Niesler FB, Zimmer B, Ishigami I *et al.* (2016) Three-dimensional-printed gas dynamic virtual nozzles for x-ray laser sample delivery. *Opt Express* **24**, 11515–11530.
51 Oberthuer D, Knoska J, Wiedorn MO, Beyerlein KR, Bushnell DA, Kovaleva EG, Heymann M, Gumprecht L, Kirian RA, Barty A *et al.* (2017) Double-flow focused liquid injector for efficient serial femtosecond crystallography. *Sci Rep* **7**, 44628.
52 Monteiro DCF, Vakili M, Harich J, Sztucki M, Meier SM, Horrell S, Josts I & Trebbin M (2019) A microfluidic flow-focusing device for low sample consumption serial synchrotron crystallography experiments in liquid flow. *J Synchrot Radiat* **26**, 406–412.
53 Weierstall U, James D, Wang C, White TA, Wang D, Liu W, Spence JC, Bruce Doak R, Nelson G, Fromme P *et al.* (2014) Lipidic cubic phase injector facilitates membrane protein serial femtosecond crystallography. *Nat Commun* **5**, 3309.
54 Johansson LC, Arnlund D, Katona G, White TA, Barty A, DePonte DP, Shoeman RL, Wickstrand C, Sharma A, Williams GJ *et al.* (2013) Structure of a photosynthetic reaction centre determined by serial femtosecond crystallography. *Nat Commun* **4**, 2911.
55 Nam KH (2019) Sample delivery media for serial crystallography. *Int J Mol Sci* **20**, 1094.
56 Liu Z, Guu TS, Cao J, Li Y, Cheng L, Tao YJ & Zhang J (2016) Structure determination of a human virus by the combination of cryo-EM and X-ray crystallography. *Biophys Rep* **2**, 55–68.
57 Zhu L, Weierstall U, Cherezov V & Liu W (2016) Serial femtosecond crystallography of membrane proteins. *Adv Exp Med Biol* **922**, 151–160.
58 Landau EM & Rosenbusch JP (1996) Lipidic cubic phases: a novel concept for the crystallization of membrane proteins. *Proc Natl Acad Sci USA* **93**, 14532–14535.
59 Rasmussen SGF, DeVree BT, Zou YZ, Kruse AC, Chung KY, Kobilka TS, Thian FS, Chae PS, Pardon E, Calinski D *et al.* (2011) Crystal structure of the beta (2) adrenergic receptor-Gs protein complex. *Nature* **477**, 549–U311.
60 Rosenbaum DM, Cherezov V, Hanson MA, Rasmussen SGF, Thian FS, Kobilka TS, Choi HJ, Yao XJ, Weis WI, Stevens RC *et al.* (2007) GPCR engineering yields high-resolution structural insights into beta(2)-adrenergic receptor function. *Science* **318**, 1266–1273.
61 Thal DM, Vuckovic Z, Draper-Joyce CJ, Liang YL, Glukhova A, Christopoulos A & Sexton PM (2018) Recent advances in the determination of G protein-coupled receptor structures. *Curr Opin Struct Biol* **51**, 28–34.
62 Ishchenko A, Gati C & Cherezov V (2018) Structural biology of G protein-coupled receptors: new opportunities from XFELs and cryoEM. *Curr Opin Struct Biol* **51**, 44–52.
63 Che T, Majumdar S, Zaidi SA, Ondachi P, McCorvy JD, Wang S, Mosier PD, Uprety R, Vardy E, Krumm BE *et al.* (2018) Structure of the nanobody-stabilized active state of the kappa opioid receptor. *Cell* **172**, 55–67.e15.
64 Audet M, White KL, Breton B, Zarzycka B, Han GW, Lu Y, Gati C, Batyuk A, Popov P, Velasquez J *et al.* (2019) Crystal structure of misoprostol bound to the labor inducer prostaglandin E2 receptor. *Nat Chem Biol* **15**, 11–17.
65 Stauch B, Johansson LC, McCorvy JD, Patel N, Han GW, Huang XP, Gati C, Batyuk A, Slocum ST, Ishchenko A *et al.* (2019) Structural basis of ligand recognition at the human MT1 melatonin receptor. *Nature* **569**, 284–288.

66 Liu W, Wacker D, Gati C, Han GW, James D, Wang DJ, Nelson G, Weierstall U, Katritch V, Barty A *et al.* (2013) Serial femtosecond crystallography of G protein-coupled receptors. *Science* **342**, 1521–1524.
67 Liu W, Wacker D, Wang C, Abola E & Cherezov V (2014) Femtosecond crystallography of membrane proteins in the lipidic cubic phase. *Philos Trans R Soc B-Biol Sci* **369**, 20130314.
68 Ishchenko A, Cherezov V & Liu W (2016) Preparation and delivery of protein microcrystals in lipidic cubic phase for serial femtosecond crystallography. *J Vis Exp*, e54463.
69 Sugahara M, Mizohata E, Nango E, Suzuki M, Tanaka T, Masudala T, Tanaka R, Shimamura T, Tanaka Y, Suno C *et al.* (2015) Grease matrix as a versatile carrier of proteins for serial crystallography. *Nat Methods* **12**, 61–63.
70 Conrad CE, Basu S, James D, Wang D, Schaffer A, Roy-Chowdhury S, Zatsepin NA, Aquila A, Coe J, Gati C *et al.* (2015) A novel inert crystal delivery medium for serial femtosecond crystallography. *IUCrJ* **2**, 421–430.
71 Lawrence RM, Conrad CE, Zatsepin NA, Grant TD, Liu HG, James D, Nelson G, Subramanian G, Aquila A, Hunter MS *et al.* (2015) Serial femtosecond X-ray diffraction of enveloped virus microcrystals. *Struct Dyn*, **2**, 041720.
72 Martin-Garcia JM, Conrad CE, Nelson G, Stander N, Zatsepin NA, Zook J, Zhu L, Geiger J, Chun E, Kissick D *et al.* (2017) Serial millisecond crystallography of membrane and soluble protein microcrystals using synchrotron radiation. *IUCrJ* **4**, 439–454.
73 Sugahara M, Song C, Suzuki M, Masuda T, Inoue S, Nakane T, Yumoto F, Nango E, Tanaka R, Tono K *et al.* (2016) Oil-free hyaluronic acid matrix for serial femtosecond crystallography. *Sci Rep* **6**, 24484.
74 Park J, Park S, Kim J, Park G, Cho Y & Nam KH (2019) Polyacrylamide injection matrix for serial femtosecond crystallography. *Sci Rep* **9**, 2525.
75 Sugahara M, Nakane T, Masuda T, Suzuki M, Inoue S, Song C, Tanaka R, Nakatsu T, Mizohata E, Yumoto F *et al.* (2017) Hydroxyethyl cellulose matrix applied to serial crystallography. *Sci Rep* **7**, 703.
76 Kovacsova G, Grunbein ML, Kloos M, Barends TRM, Schlesinger R, Heberle J, Kabsch W, Shoeman RL, Doak RB & Schlichting I (2017) Viscous hydrophilic injection matrices for serial crystallography. *IUCrJ* **4**, 400–410.
77 Fromme R, Ishchenko A, Metz M, Chowdhury SR, Basu S, Boutet S, Fromme P, White TA, Barty A, Spence JC *et al.* (2015) Serial femtosecond crystallography of soluble proteins in lipidic cubic phase. *IUCrJ* **2**, 545–551.
78 Lomelino CL, Kim JK, Lee C, Lim SW, Andring JT, Mahon BP, Chung M, Kim CU & McKenna R (2018) Carbonic anhydrase II microcrystals suitable for XFEL studies. *Acta Crystallogr F-Struct Biol Commun* **74**, 327–330.
79 Nogly P, James D, Wang DJ, White TA, Zatsepin N, Shilova A, Nelson G, Liu HG, Johansson L, Heymann M *et al.* (2015) Lipidic cubic phase serial millisecond crystallography using synchrotron radiation. *IUCrJ* **2**, 168–176.
80 Nogly P, Panneels V, Nelson G, Gati C, Kimura T, Milne C, Milathianaki D, Kubo M, Wu WT, Conrad C *et al.* (2016) Lipidic cubic phase injector is a viable crystal delivery system for time-resolved serial crystallography. *Nat Commun* **7**, 12314.
81 Sierra RG, Laksmono H, Kern J, Tran R, Hattne J, Alonso-Mori R, Lassalle-Kaiser B, Glockner C, Hellmich J, Schafer DW *et al.* (2012) Nanoflow electrospinning serial femtosecond crystallography. *Acta Crystallogr D Biol Crystallogr* **68**, 1584–1587.
82 Sierra RG, Gati C, Laksmono H, Dao EH, Gul S, Fuller F, Kern J, Chatterjee R, Ibrahim M, Brewster AS *et al.* (2016) Concentric-flow electrokinetic injector enables serial crystallography of ribosome and photosystem II. *Nat Methods* **13**, 59–62.
83 Bielecki J, Hantke MF, Daurer BJ, Reddy HKN, Hasse D, Larsson DSD, Gunn LH, Svenda M, Munke A, Sellberg JA *et al.* (2019) Electrospray sample injection for single-particle imaging with x-ray lasers. *Sci Adv* **5**, eaav8801.
84 Oberthur D (2018) Biological single-particle imaging using XFELs - towards the next resolution revolution. *IUCrJ* **5**, 663–666.
85 Rose M, Bobkov S, Ayyer K, Kurta RP, Dzhigaev D, Kim YY, Morgan AJ, Yoon CH, Westphal D, Bielecki J *et al.* (2018) Single-particle imaging without symmetry constraints at an X-ray free-electron laser. *IUCrJ* **5**, 727–736.
86 Reddy HKN, Yoon CH, Aquila A, Awel S, Ayyer K, Barty A, Berntsen P, Bielecki J, Bobkov S, Bucher M *et al.* (2017) Coherent soft X-ray diffraction imaging of coliphage PR772 at the Linac coherent light source. *Scientific Data* **4**, 170079.
87 Munke A, Andreasson J, Aquila A, Awel S, Ayyer K, Barty A, Bean RJ, Berntsen P, Bielecki J, Boutet S *et al.* (2016) Coherent diffraction of single Rice Dwarf virus particles using hard X-rays at the Linac Coherent Light Source. *Sci Data* **3**, 160064.
88 Kirian RA, Awel S, Eckerskorn N, Fleckenstein H, Wiedorn M, Adriano L, Bajt S, Barthelmess M, Bean R, Beyerlein KR *et al.* (2015) Simple convergent-nozzle aerosol injector for single-particle diffractive imaging with X-ray free-electron lasers. *Struct Dyn* **2**, 041717.
89 Bogan MJ, Benner WH, Boutet S, Rohner U, Frank M, Barty A, Seibert MM, Maia F, Marchesini S, Bajt S *et al.* (2008) Single particle X-ray diffractive imaging. *Nano Lett* **8**, 310–316.

90 Hantke MF, Bielecki J, Kulyk O, Westphal D, Larsson DSD, Svenda M, Reddy HKN, Kirian RA, Andreasson J, Hajdu J *et al.* (2018) Rayleigh-scattering microscopy for tracking and sizing nanoparticles in focused aerosol beams. *IUCrJ* **5**, 673–680.
91 Seibert MM, Ekeberg T, Maia FR, Svenda M, Andreasson J, Jonsson O, Odic D, Iwan B, Rocker A, Westphal D *et al.* (2011) Single mimivirus particles intercepted and imaged with an X-ray laser. *Nature* **470**, 78–81.
92 Loh ND, Hampton CY, Martin AV, Starodub D, Sierra RG, Barty A, Aquila A, Schulz J, Lomb L, Steinbrener J *et al.* (2012) Fractal morphology, imaging and mass spectrometry of single aerosol particles in flight. *Nature* **486**, 513–517.
93 van der Schot G, Svenda M, Maia FR, Hantke M, DePonte DP, Seibert MM, Aquila A, Schulz J, Kirian R, Liang M *et al.* (2015) Imaging single cells in a beam of live cyanobacteria with an X-ray laser. *Nat Commun* **6**, 5704.
94 Hantke MF, Hasse D, Maia FRNC, Ekeberg T, John K, Svenda M, Loh ND, Martin AV, Timneanu N, Larsson DSD *et al.* (2014) High-throughput imaging of heterogeneous cell organelles with an X-ray laser. *Nat Photonics* **8**, 943–949.
95 Awel S, Kirian RA, Wiedorn MO, Beyerlein KR, Roth N, Horke DA, Oberthur D, Knoska J, Mariani V, Morgan A *et al.* (2018) Femtosecond X-ray diffraction from an aerosolized beam of protein nanocrystals. *J Appl Crystallogr* **51**, 133–139.
96 Mancuso AP, Aquila A, Batchelor L, Bean RJ, Bielecki J, Borchers G, Doerner K, Giewekemeyer K, Graceffa R, Kelsey OD *et al.* (2019) The single particles. Clusters and biomolecules and serial femtosecond crystallography instrument of the European XFEL: initial installation. *J Synchrot Radiat* **26**, 660–676.
97 Wu P, Noland C, Ultsch M, Edwards B, Harris D, Mayer R & Harris SF (2016) Developments in the implementation of acoustic droplet ejection for protein crystallography. *J Lab Autom* **21**, 97–106.
98 Ericson DL, Yin X, Scalia A, Samara YN, Stearns R, Vlahos H, Ellson R, Sweet RM & Soares AS (2016) acoustic methods to monitor protein crystallization and to detect protein crystals in suspensions of agarose and lipidic cubic phase. *J Lab Autom* **21**, 107–114.
99 Roessler CG, Agarwal R, Allaire M, Alonso-Mori R, Andi B, Bachega JFR, Bommer M, Brewster AS, Browne MC, Chatterjee R *et al.* (2016) Acoustic injectors for drop-on-demand serial femtosecond crystallography. *Structure* **24**, 631–640.
100 Fuller FD, Gul S, Chatterjee R, Burgie ES, Young ID, Lebrette H, Srinivas V, Brewster AS, Michels-Clark T, Clinger JA *et al.* (2017) Drop-on-demand sample delivery for studying biocatalysts in action at X-ray free-electron lasers. *Nat Methods* **14**, 443–449.
101 Kern J, Chatterjee R, Young ID, Fuller FD, Lassalle L, Ibrahim M, Gul S, Fransson T, Brewster AS, Alonso-Mori R *et al.* (2018) Structures of the intermediates of Kok's photosynthetic water oxidation clock. *Nature* **563**, 421–425.
102 Oghbaey S, Sarracini A, Ginn HM, Pare-Labrosse O, Kuo A, Marx A, Epp SW, Sherrell DA, Eger BT, Zhong Y *et al.* (2016) Fixed target combined with spectral mapping: approaching 100% hit rates for serial crystallography. *Acta Crystallogr D Struct Biol* **72**, 944–955.
103 Cohen AE, Soltis SM, Gonzalez A, Aguila L, Alonso-Mori R, Barnes CO, Baxter EL, Brehmer W, Brewster AS, Brunger AT *et al.* (2014) Goniometer-based femtosecond crystallography with X-ray free electron lasers. *Proc Natl Acad Sci USA* **111**, 17122–17127.
104 Hirata K, Shinzawa-Itoh K, Yano N, Takemura S, Kato K, Hatanaka M, Muramoto K, Kawahara T, Tsukihara T, Yamashita E *et al.* (2014) Determination of damage-free crystal structure of an X-ray-sensitive protein using an XFEL. *Nat Methods* **11**, 734–736.
105 Halsted TP, Yamashita K, Hirata K, Ago H, Ueno G, Tosha T, Eady RR, Antonyuk SV, Yamamoto M & Hasnain SS (2018) An unprecedented dioxygen species revealed by serial femtosecond rotation crystallography in copper nitrite reductase. *IUCrJ* **5**, 22–31.
106 Hunter MS, Segelke B, Messerschmidt M, Williams GJ, Zatsepin NA, Barty A, Benner WH, Carlson DB, Coleman M, Graf A *et al.* (2014) Fixed-target protein serial microcrystallography with an x-ray free electron laser. *Sci Rep* **4**, 6026.
107 Coquelle N, Brewster AS, Kapp U, Shilova A, Weinhausen B, Burghammer M & Colletier JP (2015) Raster-scanning serial protein crystallography using micro- and nano-focused synchrotron beams. *Acta Crystallogr Sect D-Struct Biol* **71**, 1184–1196.
108 Roedig P, Vartiainen I, Duman R, Panneerselvam S, Stube N, Lorbeer O, Warmer M, Sutton G, Stuart DI, Weckert E *et al.* (2015) A micro-patterned silicon chip as sample holder for macromolecular crystallography experiments with minimal background scattering. *Sci Rep* **5**, 10451.
109 Roedig P, Duman R, Sanchez-Weatherby J, Vartiainen I, Burkhardt A, Warmer M, David C, Wagner A & Meents A (2016) Room-temperature macromolecular crystallography using a micro-patterned silicon chip with minimal background scattering. *J Appl Crystallogr* **49**, 968–975.
110 Murray TD, Lyubimov AY, Ogata CM, Vo H, Uervirojnangkoorn M, Brunger AT & Berger JM (2015) A high-transparency, micro-patternable chip for X-ray diffraction analysis of microcrystals under native growth conditions. *Acta Crystallogr Sect D-Struct Biol* **71**, 1987–1997.

111 Sui S, Wang Y, Kolewe KW, Srajer V, Henning R, Schiffman JD, Dimitrakopoulos C & Perry SL (2016) Graphene-based microfluidics for serial crystallography. *Lab Chip* **16**, 3082–3096.
112 Roedig P, Ginn HM, Pakendorf T, Sutton G, Harlos K, Walter TS, Meyer J, Fischer P, Duman R, Vartiainen I *et al*. (2017) High-speed fixed-target serial virus crystallography. *Nat Methods* **14**, 805–810.
113 Doak RB, Kovacs GN, Gorel A, Foucar L, Barends TRM, Grunbein ML, Hilpert M, Kloos M, Roome CM, Shoeman RL *et al*. (2018) Crystallography on a chip - without the chip: sheet-on-sheet sandwich. *Acta Crystallogr Sect D Struct Biol* **74**, 1000–1007.
114 Schulz EC, Mehrabi P, Muller-Werkmeister HM, Tellkamp F, Jha A, Stuart W, Persch E, De Gasparo R, Diederich F, Pai EF *et al*. (2018) The hit-and-return system enables efficient time-resolved serial synchrotron crystallography. *Nat Methods* **15**, 901–904.
115 Baxter EL, Aguila L, Alonso-Mori R, Barnes CO, Bonagura CA, Brehmer W, Brunger AT, Calero G, Caradoc-Davies TT, Chatterjee R *et al*. (2016) High-density grids for efficient data collection from multiple crystals. *Acta Crystallogr Sect D-Struct Biol* **72**, 2–11.
116 Mathews II, Allison K, Robbins T, Lyubimov AY, Uervirojnangkoorn M, Brunger AT, Khosla C, DeMirci H, McPhillips SE, Hollenbeck M *et al*. (2017) The conformational flexibility of the acyltransferase from the disorazole polyketide synthase is revealed by an X-ray free-electron laser using a room-temperature sample delivery method for serial crystallography. *Biochemistry* **56**, 4751–4756.
117 Axford D, Aller P, Sanchez-Weatherby J & Sandy J (2016) Applications of thin-film sandwich crystallization platforms. *Acta Crystallogr F Struct Biol Commun* **72**, 313–319.
118 Gicquel Y, Schubert R, Kapis S, Bourenkov G, Schneider T, Perbandt M, Betzel C, Chapman HN & Heymann M (2018) Microfluidic chips for *in situ* crystal X-ray diffraction and *in situ* dynamic light scattering for serial crystallography. *J Vis Exp*, e57133.
119 Ren Z, Ayhan M, Bandara S, Bowatte K, Kumarapperuma I, Gunawardana S, Shin H, Wang C, Zeng XT & Yang XJ (2018) Crystal-on-crystal chips for in situ serial diffraction at room temperature. *Lab Chip* **18**, 2246–2256.
120 Beyerlein KR, Dierksmeyer D, Mariani V, Kuhn M, Sarrou I, Ottaviano A, Awel S, Knoska J, Fuglerud S, Jonsson O *et al*. (2017) Mix-and-diffuse serial synchrotron crystallography. *IUCrJ* **4**, 769–777.
121 Lomb L, Steinbrener J, Bari S, Beisel D, Berndt D, Kieser C, Lukat M, Neef N & Shoeman RL (2012) An anti-settling sample delivery instrument for serial femtosecond crystallography. *J Appl Crystallogr* **45**, 674–678.